Research Article

Ülkü Bayhan*

Ab initio study of fundamental properties of $XInO_3$ (X = K, Rb, Cs) perovskites

https://doi.org/10.1515/chem-2022-0268
received November 24, 2022; accepted December 15, 2022

Abstract: The structural, elastic, anisotropic, and lattice dynamical properties of cubic perovskite compounds $XInO_3$ (X = K, Rb, and Cs) are investigated using first-principles calculations. Electronic band structures and state densities revealed that the electronic nature of the studied materials exhibited half-metallicity properties. The existence of O p–d states close to the Fermi level contributes to the half-metallic properties. Moreover, polycrystalline properties, such as bulk, Young, and shear moduli and Pugh and Poisson ratios, have been determined. As a result of these characteristics, the compounds under consideration exhibited ductility behavior. As far as is known, since this is the first study of $XInO_3$ (X = K, Rb, and Cs) compounds, this work sheds light on future works.

Keywords: DFT, $XInO_3$ (X = K, Rb, and Cs) perovskite compounds, half-metallicity

1 Introduction

Researchers' favorites and prominent in all areas of material sciences are perovskites, which are found in the world's natural formations and whose effective and rare physical features have lately been recognized. Although it is referred to as perovskite, the calcium–titanium–oxygen complex $CaTiO_3$ is also used to characterize it. The first man who finds this mineral was the Russian mineralogist Gustav Rose. In 1839, researchers recognized other minerals with a comparable crystalline structure called perovskites. These new compounds, which have a general structure of type ABC_3, were discovered by Russian mineralogists and named Perovskite in honor of Lev Perovski (1792–1856). Perovskite materials' interesting and surprising properties are newly recognized, and they are being pursued by researchers with rising momentum [1–3].

The challenge of being able to store energy generated and utilize it later is a matter of importance when resolving energy problems persists. New materials, particularly perovskite oxides as electrochemical energy materials, offer a great advantage to be utilized as a possible host or carrier for applications. This theoretical study covers the latest progress of one group example of ABO_3 perovskite oxides, with no more information in the literature. In this study, the structural, elastic, anisotropic elastic, electronic, and lattice dynamical properties of $XInO_3$ (X = K, Rb, and Cs) were examined using density functional theory (DFT) implemented by the *Vienna ab initio simulation package* (VASP). The lattice constant, bulk, Young's, and shear moduli, and Poisson's ratio have been investigated. Current compounds are stable, both mechanically and dynamically. The calculations revealed that these compounds retain some brittleness while also exhibiting ductility. The material may show bending behavior. With this feature, it can be said that it has the potential to be a new material that can be used in eco-friendly wearable technologies [3–6].

2 Calculation methods

DFT calculations on $XInO_3$ (X = K, Rb, and Cs) perovskites were performed using the VASP [7,8]. Electron–ion interaction was handled by the projector-augmented wave method with a 500 eV cutoff energy [9,10]. The Perdew–Burke–Ernzerhof functional with generalized gradient approximation has been used for exchange-correlation in electron–electron interactions [11]. For the compounds investigated, gamma-centered 16 × 16 × 16 with an automatic k-mesh has been performed. Methfessel–Paxton smearing has been addressed to oneself as 0.025 eV [12]. The convergence criteria were taken up as 10^{-6} eV Å^{-1} and 10^{-8} eV, respectively.

* **Corresponding author: Ülkü Bayhan,** Department of Physics, Burdur Mehmet Akif Ersoy University, Burdur, Turkey,
e-mail: ubayhan@mehmetakif.edu.tr
ORCID: Ülkü Bayhan 0000-0003-3793-3130

3 Results and discussions

The $XInO_3$ (X = K, Rb, and Cs) perovskites crystallize/take shape in space group $Pm\bar{3}m$. The *Wyckoff* locations *1a* (0.0, 0.0, 0.0) for the X atoms, *1b* (0.5, 0.5, 0.5) for the In, and *3c* (0.0, 0.5, 0.5), (0.5, 0.0, 0.5), and (0.5, 0.5, 0.0) for the three O atoms, respectively, are where the atoms in compounds under investigation are located. Figure 1 details the structure of the current compounds.

Table 1 accounts for the calculated lattice constants (a in Å), volume (V in $Å^3$), density (ρ in $g\,cm^{-3}$), and formation energy (ΔH_f in eV $atom^{-1}$).

It can be concluded that the lattice constants, volume, and density have increased for the investigated compounds, as categorized in Table 1. Furthermore, the results of the formation energy, calculated by using equation (1), have demonstrated that those compounds can be both synthesizable and thermodynamically stable:

$$\Delta H_f = E^{\text{Total}}_{XInO_3} - (E^{\text{Total}}_{X} + E^{\text{Total}}_{In} + (3 \times E^{\text{Total}}_{O})). \quad (1)$$

Table 1: Calculated structural properties for $XInO_3$ (X = K, Rb, and Cs)

Compounds	a (Å)	V ($Å^3$)	ρ ($g\,cm^{-3}$)	ΔH_f (eV $atom^{-1}$)
$KInO_3$	4.293	79.101	4.239	−1.473
$RbInO_3$	4.336	81.512	5.058	−1.358
$CsInO_3$	4.395	84.915	5.783	−1.271

Table 2: Calculated elastic constants (C_{ij} in GPa), bulk, shear, and Young's moduli (B, G, and E in GPa), B/G, G/B, Poisson's ratio (v), and Vicker's hardness (H_f in GPa)

Compounds	$KInO_3$	$RbInO_3$	$CsInO_3$
C_{11}	157.406	144.325	117.118
C_{12}	40.359	46.484	48.490
C_{44}	1.424	10.191	16.180
B	79.375	79.097	71.366
G	37.788	56.096	59.789
E	13.300	20.298	21.975
B/G	5.968	3.897	3.248
G/B	0.168	0.257	0.308
v	0.421	0.382	0.360
H_f	0.754	1.651	2.149

3.1 Mechanical properties

Either conceptual or portable applications require mechanical characteristics, which are both beneficial and essential. As a result, it is necessary to compute the mechanical properties of the compounds considered. Therefore, current compounds must adhere to the Born stability conditions [13], which are as follows: $C_{11} - C_{12} > 0$; $C_{11} + 2C_{12} > 0$; $C_{44} > 0$. Table 2 depicts the calculated elastic constants (C_{ij} in GPa), bulk, shear, and Young's moduli (B, G, and E in GPa), B/G, G/B, Poisson's ratio, and Vicker's hardness (H_f in GPa).

It is possible to see that the compounds meet Born stability criteria, and those compounds are mechanically stable. Thus, they are suitable for conceptual or portable applications. The elastic constants can be used to express the polycrystalline properties such as bulk (B), shear (G), Young's moduli (E), B/G, G/B, Poisson's ratio (v), and Vicker's hardness (H_f), and they are calculated by using equations (2)–(6), respectively. In equations (2) and (3), the Voigt [14] and Reuß [15] approximations are symbolized as subscripts V and R, respectively. The protection of the compound to volume modification under applied hydrostatic pressure could be referred to as the bulk modulus, as it is commonly known in [16]. As already concluded from Table 2, $KInO_3$ has the highest bulk modulus, while $CsInO_3$ has the lowest of the investigated compounds. The relationship between shear stress and shear strain can be used to discover the shear modulus, also known as elastic shear stiffness [17]. As can be seen

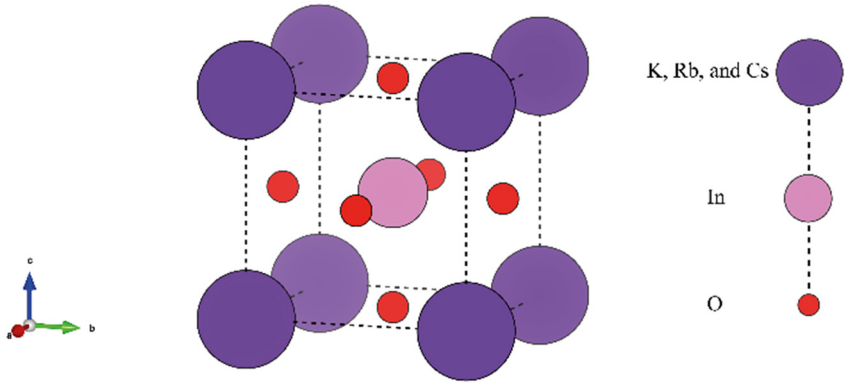

Figure 1: The structure of $XInO_3$ (X = K, Rb, and Cs) compounds.

in Table 2, $CsInO_3$ has the highest shear modulus, whereas $KInO_3$ has the lowest one. As an indicator of elasticity, Young's modulus is determined by stress-to-strain ratios caused by uniaxial deformation [18]. Among the investigated compounds, $KInO_3$ has the lowest Young's modulus, while $CsInO_3$ has the highest. The B/G ratio, an essential parameter for determining the consistency of the compound, indicates brittleness if it is less than 1.75; otherwise, it indicates ductility. As can be noted in Table 2, the computed results of the B/G are larger than the vital value (1.75); therefore, it is possible to say that current compounds have shown ductility characteristics within observations [19]. The ratio G/B, another serious criterion, helps predict the bonding peculiarities of compounds and is directly related to the bonding nature of compounds. The ratio G/B, which is another decisive criterion owing to helping predict the bonding peculiarity of compounds, identifies that if it is around 0.6, the compound has a predominantly ionic bonding nature. In contrast, if this ratio is about 1.1, the compound has demonstrated covalent bonding predominantly. Since the G/B ratios of these compounds are less than 0.6, the investigated compounds have exhibited dominantly ionic bonding characteristics, as is seen in Table 2 [20]. Analogous to G/B, the Poisson's ratio is useful for describing bonding properties. Ionic and covalent bonding compounds have Poisson's ratios of about 0.25 and 0.1, respectively [21]. As can be seen in Table 2, Poisson's ratios for the studied compounds are larger than 0.25; hence, the present compounds have indicated ionic bonding in harmony with G/B results. Vicker's hardness, the last specification in Table 2, was computed utilizing the semiempirical equation proposed by Tian et al. [22] standing on G/B known as Pugh's modulus, as follows:

$$B = \frac{B_V + B_R}{2}, \tag{2}$$

$$G = \frac{G_V + G_R}{2}, \tag{3}$$

$$E = \frac{9BG}{G + 3B}, \tag{4}$$

$$\nu = \frac{1}{2}\left[\frac{\left(B - \frac{2G}{3}\right)}{\left(B + \frac{G}{3}\right)}\right], \tag{5}$$

$$H_v = 0.92k^{1.137}G^{0.708}, \quad k = G/B. \tag{6}$$

In all aspects, as concluded from Vicker's hardness results, these compounds are not so hard materials. This behavior makes the compounds ductile.

3.2 Anisotropic properties

Anisotropic behaviors are beneficial for determining microcracks in the compounds. In crystals with cubic symmetry, the Zener anisotropy (A), given in equation (7), and maximum–minimum polycrystalline properties are enough to explain this nature. Table 3 depicts these quantities.

$$A = \frac{2C_{44}}{C_{11} - C_{12}}. \tag{7}$$

The considered compounds have exhibited anisotropic properties due to the A being far from 1. The A measures that the compounds are far from isotropic, as is known. As can be seen in Table 3, $KInO_3$ has largest anisotropy, whereas $CsInO_3$ has the smallest. Furthermore, with the exception of linear compressibility, analyzed polycrystalline properties have inferred an anisotropic nature. The observed isotropic characteristics of linear compressibility are caused by cubic symmetry. The calculated Poisson ratios of these compounds show that they exceed the theoretical upper bound [23,24]. As a result, these compounds are likely to exhibit significant elastic deformation under minimally applied strain. In addition, the current results are visible in Figure 2. The parameters for different materials for different purposes have also been investigated, and interesting results have been found [25–36].

The thermal characteristics of a compound, such as melting point and thermal conductivity, can be determined using the Debye temperature (θ_D), which is denoted by equation (11), where the Planck constant is h, the Boltzmann constant is k_B, the Avogadro number is N_A, the density is ρ, the number of atoms in the unit cell is n, and the molecular mass of the compound is M. The compound has a high melting point and thermal

Table 3: The calculated Zener ratio (A) and max–min points of Young's modulus (E in GPa), linear compressibility (β in TPa^{-1}), shear modulus (G in GPa), and Poisson's ratio (ν)

		$KInO_3$	$RbInO_3$	$CsInO_3$
A		0.024	0.208	0.472
Young's modulus	E_{min}	4.247	29.314	45.129
	E_{max}	140.930	121.680	88.722
Linear compressibility	$\beta_{min} = \beta_{max}$	4.200	4.214	4.671
Shear modulus	G_{min}	1.424	10.191	16.180
	G_{max}	58.523	48.920	34.314
Poisson's ratio	ν_{min}	0.008	0.072	0.170
	ν_{max}	0.968	0.775	0.590

conductivity when the θ_D is high. Among handled compounds, $RbInO_3$ has the highest melting point and thermal conductivity due to large θ_D, as considered in Table 4.

$$V_l = \left(\frac{3B + 4G}{4\rho}\right)^{0.5}, \tag{8}$$

$$V_t = \left(\frac{G}{\rho}\right)^{\frac{1}{2}}, \tag{9}$$

$$V_m = \left[\frac{1}{3}\left(\frac{2}{V_t^3} + \frac{1}{V_l^3}\right)\right]^{-\frac{1}{3}}, \tag{10}$$

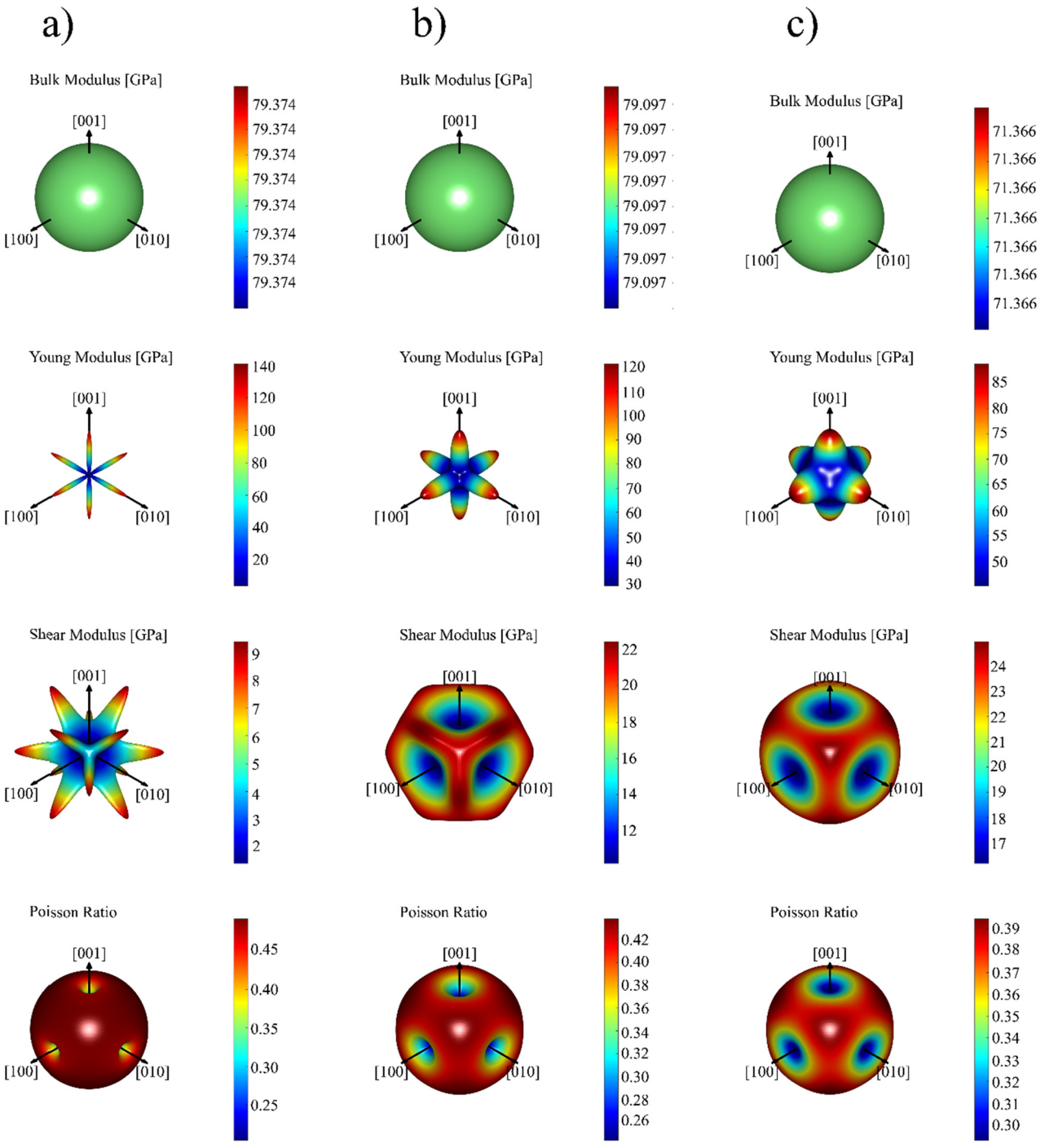

Figure 2: The graphical notation of polycrystalline properties for $XInO_3$ (X = K, Rb, and Cs) compounds. (a) $KInO_3$, (b) $RbInO_3$, and (c) $CsInO_3$.

Table 4: The longitudinal (V_l), transverse (V_t), and average (V_m) wave velocities and Debye temperature (θ_D) for $XInO_3$ (X = K, Rb, and Cs) compounds

Compounds	V_l (m s^{-1})	V_t (m s^{-1})	V_m (m s^{-1})	θ_D (K)
$KInO_3$	4786.415	1771.347	2010.841	238.479
$RbInO_3$	4581.397	2003.284	2262.097	265.604
$CsInO_3$	4172.218	1949.357	2194.765	254.210

$$\theta_D = \frac{h}{k_B}\left[\frac{3n}{4\pi}\left(\frac{N_A\rho}{M}\right)\right]^{\frac{1}{3}} \times V_m. \tag{11}$$

3.3 Electronic properties

The electronic behavior of handled compounds could be revealed by calculating their electronic properties. Figure 3 presents the band structures and, relatedly, the density of states (DOSs) for $XInO_3$ (X = K, Rb, and Cs) compounds along with respective symmetry lines.

The investigated compounds have exhibited half-metallic properties. Current computations show that the spin-up status' semiconductor behavior, whereas the spin-down state has a metallic nature owing to some bands originating from O p–d occurrences, as seen in Figure 4, reaching the Fermi level and giving the compound a half-metallic character by reducing the gap.

It is possible to observe that the X-atom contributions are about −10 eV for K, −8 eV for Rb, and −5 eV for Cs, respectively, according to Figure 4. In addition to the contribution of roughly −15 eV, the O makes a contribution that lends half-metallicity nature, while the In makes no significant contribution. Moreover, as a result of spin-polarized calculations, each compound investigated has a magnetic moment of about $2\mu_B$.

3.4 Lattice dynamical and thermodynamical properties

Figure 5 depicts the phonon curves and, relatedly, the PDOS for the respective compound under investigation. Owing to the five atoms that make up their unit cell, there are likely 15 phonon branches, as is consistent with observations. Twelve of these branches are optical modes, whereas the remaining branches are acoustic modes. The considered compounds are also dynamically stable since no soft mode has been observed.

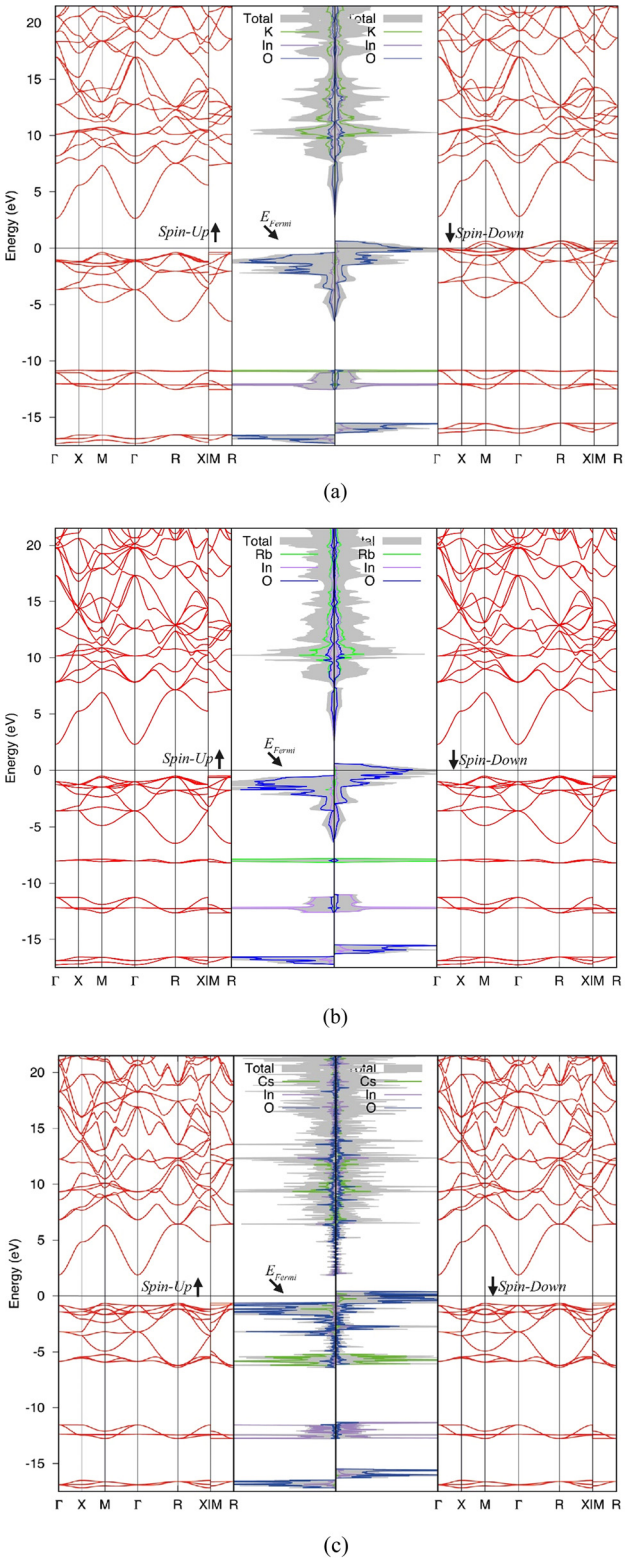

Figure 3: The band structures and related DOSs for $XInO_3$ (X = K (a), Rb (b), and Cs (c)) compounds.

Figure 6 demonstrates the thermal properties of considered compounds. These representations deal with the relationship between temperature and free energy,

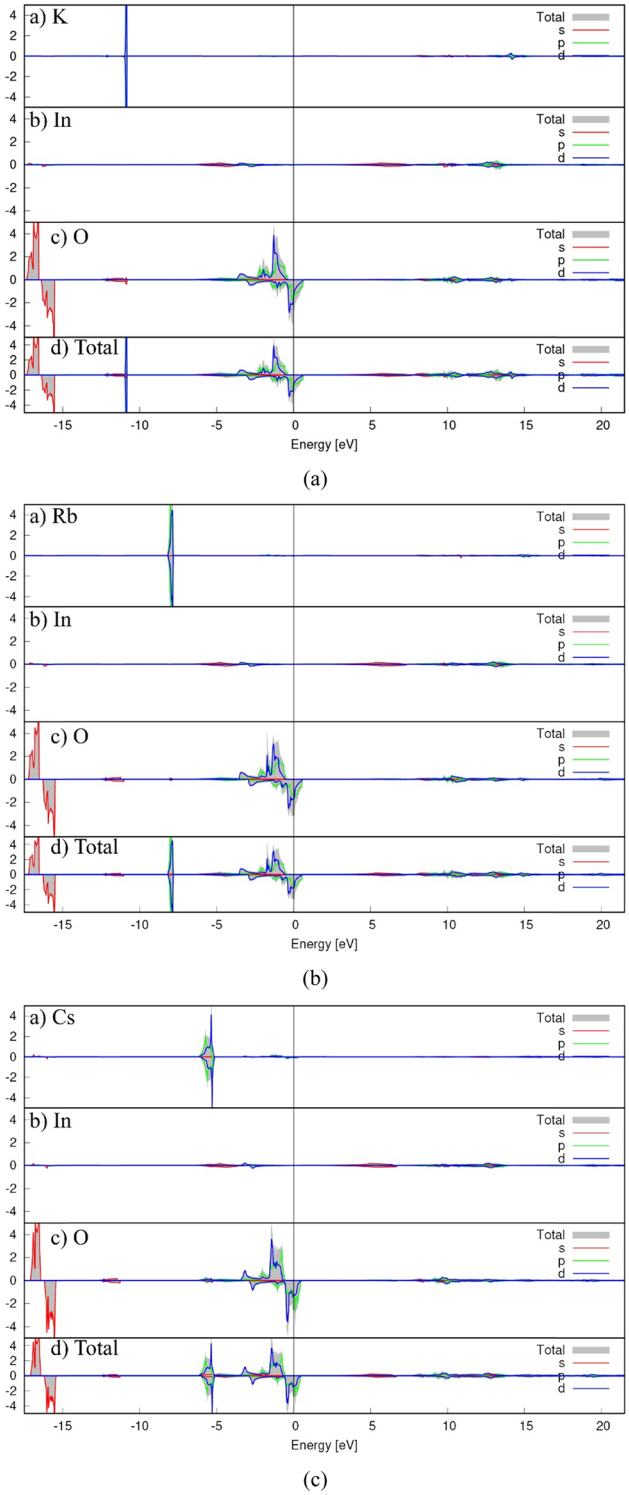

Figure 4: The partial DOSs (PDOSs) for $XInO_3$ (X = K (a), Rb (b), and Cs (c)) compounds.

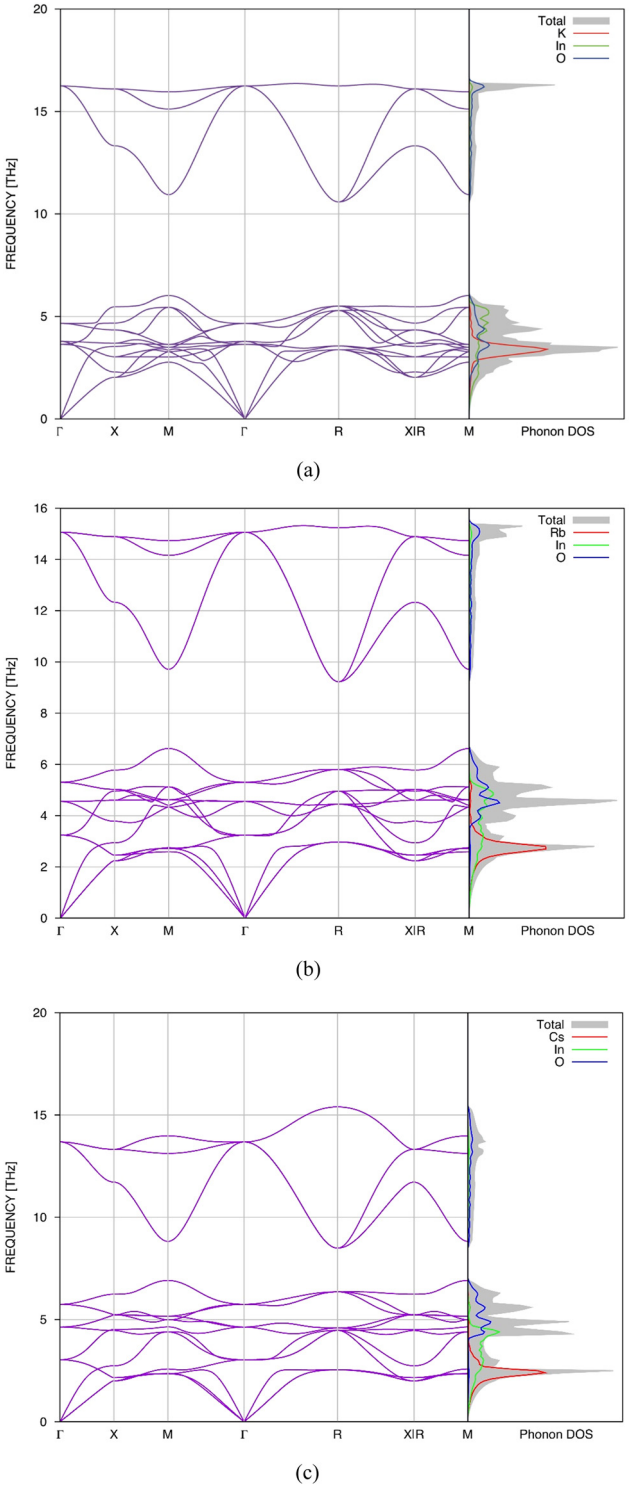

Figure 5: The calculated phonon dispersion curves and, relatedly, PDOS for $XInO_3$ (X = K (a), Rb (b), and Cs (c)) compounds.

entropy, and heat capacity. In addition, it is evident that as temperature rises, free energy falls dramatically. Entropy, on the other hand, increases when the temperature rises. The heat capacity grows dramatically at low temperatures and reaches the Dulong–Petit limit, which is constant at high temperatures.

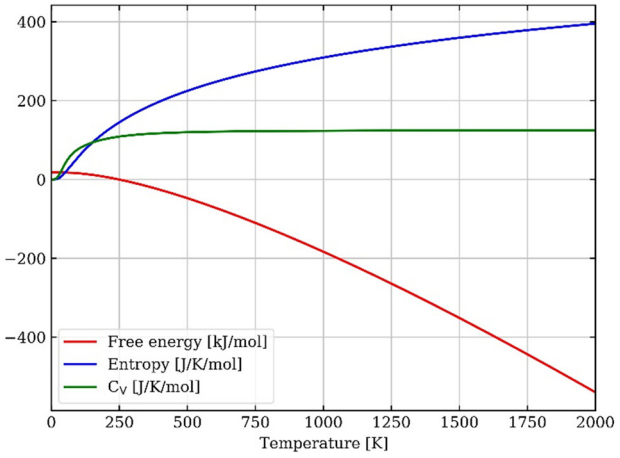

(a)

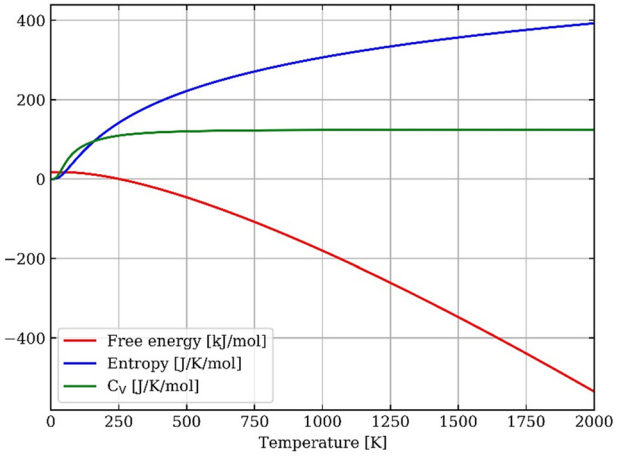

(b)

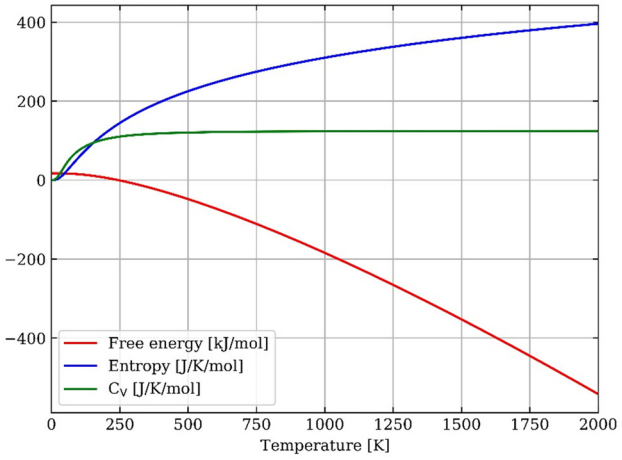

(c)

Figure 6: The calculated thermal properties for $XInO_3$ (X = K (a), Rb (b), and Cs (c)) compounds.

4 Conclusion

The objective of this examination was to reveal the structural, elastic, anisotropic, electronic, lattice dynamical, and thermal properties of $XInO_3$ (X = K, Rb, and Cs) compounds using DFT implemented in VASP 544. Moreover, the investigated compounds are both thermodynamically stable and experimentally synthesizable due to having negative formation energy. In addition, these compounds have demonstrated stable lattice dynamical properties. Since the calculated ν_{max} of these compounds is larger than the upper limit of Poisson's ratio, it is estimated that current compounds will show persistent plastic deformation under applied strain. These compounds have exhibited half-metallic behavior. Besides, they have dominant ionic characteristics. Based on our knowledge, this theoretical study, which is the first examination of investigated compounds, may provide insight into future research.

Funding information There is no funding for this article.

Conflict of interest: The author states no conflict of interest.

Ethical approval: The conducted research is not related to either human or animal use.

Data availability statement: Derived data supporting the findings of this study are available from the corresponding author on request.

References

[1] Ekmekçi M. Flexible solar cells used in self-powered wearable electronic technologies. Uşak Üniversitesi Fen ve Doğa Bilimleri Derg. 2022;6:22–33.

[2] Kim S, Van Quy H, Bark CW. Photovoltaic technologies for flexible solar cells: beyond silicon. Mater Today. Energy. 2021;19:100583.

[3] Li Q, Balilonda A, Ali A, Jose R, Zabihi F, Yang S, et al. Flexible solar yarns with 15.7% power conversion efficiency, based on electrospun perovskite composite nanofibers. Sol RRL. 2020;4(9):2000269.

[4] Ural A, Kilimci ZH. The Prediction of Chiral Metamaterial Resonance using Convolutional Neural Networks and Conventional Machine Learning Algorithms. Int J Comput Exp Sci Eng. 2021;7(3):156–63.

[5] Caymaz T, Çalışkan S, Botsalı AR. Evaluation of ergonomic conditions using fuzzy logic in a metal processing plant. Int J Comput Exp Sci Eng. 2022;8(1):19–24.
[6] Arbouz H. Modeling of a tandem solar cell structure based on CZTS and CZTSe absorber materials. Int J Comput Exp Sci Eng. 2022;8(1):14–8.
[7] Kresse G, Furthmüller J. Efficiency of ab-initio total energy calculations for metals and semiconductors using a plane-wave basis set. Comput Mater Sci. 1996;6(1):15–50.
[8] Kresse G, Furthmüller J. Efficient iterative schemes for ab initio total-energy calculations using a plane-wave basis set. Phys Rev B Condens Matter. 1996 Oct;54(16):11169–86.
[9] Blöchl PE. Projector augmented-wave method. Phys Rev B Condens Matter. 1994 Dec;50(24):17953–79.
[10] Kresse G, Joubert D. From ultrasoft pseudopotentials to the projector augmented-wave method. Phys Rev B Condens Matter. 1999;59(3):1758–75.
[11] Perdew JP, Burke K, Ernzerhof M. Generalized gradient approximation made simple. Phys Rev Lett. 1996 Oct;77(18):3865–8.
[12] Methfessel M, Paxton AT. High-precision sampling for Brillouin-zone integration in metals. Phys Rev B Condens Matter. 1989 Aug;40(6):3616–21.
[13] Li C, Wang B, Wang R, Wang H, Lu X. First-principles study of structural, elastic, electronic, and optical properties of orthorhombic $BiGaO_3$. Comput Mater Sci. 2008;42(4):614–8.
[14] Voigt W. Lehrbuch der kristallphysik: (mit ausschluss der kristalloptik). Vol. 34. BG Teubner; 1910.
[15] Reuß A. Berechnung der fließgrenze von mischkristallen auf grund der plastizitätsbedingung für einkristalleZAMM-Journal of Applied Mathematics and Mechanics. Z Angew Math Mech. 1929;9(1):49–58.
[16] Bayhan Ü, Yılmaz İ. Prediction of structural, electronic, and lattice dynamical properties of ABO_3 [A = K, Rb, Cs; B = Sn, Sb] perovskite compounds. Phys B. 2022;649:414355.
[17] Bayhan Ü, Yılmaz İ. The structural, elastic, electronic, vibrational and gravimetric hydrogen capacity properties of the perovskite type hydrides: DFT study. Preprints; 2021. doi: 10.20944/preprints202110.0269.v1.
[18] Gencer A, Yılmaz İ, Bayhan U, Surucu G. Anisotropic elastic and lattice dynamical properties of Cr_2AB MAX phases compounds. Avrupa Bilim ve Teknoloji Derg. 2019;15:351–9.
[19] Pugh SF. XCII. Relations between the elastic moduli and the plastic properties of polycrystalline pure metals. Lond Edinb Dublin Philos Mag J Sci. 1954;45(367):823–43.
[20] Saadi B. Ab initio study of fundamental properties of $XAlO_3$ (X = Cs, Rb and K) compounds. J Sci Adv Mater Devices. 2018;3(2):254–61.
[21] Bannikov VV, Shein IR, Ivanovskii AL. Electronic structure, chemical bonding and elastic properties of the first thorium-containing nitride perovskite $TaThN_3$. Phys Status Solidi Rapid Res Lett. 2007;1(3):89–91.
[22] Tian Y, Xu B, Zhao Z. Microscopic theory of hardness and design of novel superhard crystals. Int J Refract Hard Met. 2012;33:93–106.
[23] Gorodtsov VA, Lisovenko DS. Extreme values of Young's modulus and Poisson's ratio of hexagonal crystals. Mech Mater. 2019;134:1–8.
[24] Hossain MM, Ali MA, Uddin MM, Hossain MA, Rasadujjaman M, Naqib SH, et al. Influence of Se doping on recently synthesized $NaInS_{2-x}Se_x$ solid solutions for potential thermo-mechanical applications studied via first-principles method. Mater Today Commun. 2021;26:101988.
[25] ALMisned G, Baykal DS, Kilic G, Susoy G, Zakaly HM, Ene A, et al. Assessment of the usability conditions of Sb_2O_3-PbO-B_2O_3 glasses for shielding purposes in some medical radioisotope and a wide gamma-ray energy spectrum. Appl Rheol. 2022;32(1):178–89.
[26] Rwashdı QA, Waheed F, Gunoglu K, Akkurt İ. Experimental testing of the radiation shielding properties for steel. Int J Comput Exp Sci Eng. 2022;8(3):74–6.
[27] ALMisned G, Baykal DS, Kilic G, Susoy G, Zakaly HM, Ene A, et al. Determination of gamma-ray transmission factors of WO_3–TeO_2–B_2O_3 glasses using MCPX Monte Carlo code for shielding and protection purposes. Appl Rheol. 2022;32(1):166–77.
[28] Karaali R, Keven A. Evaluation of four different cogeneration cycles by using some criteria. Appl Rheol. 2022;32(1):122–37.
[29] Waheed F, İmamoğlu M, Karpuz N, Ovalıoğlu H. Simulation of neutrons shielding properties for some medical materials. Int J Comput Exp Sci Eng. 2022;8(1):5–8.
[30] Salima B, Seloua D, Djamel F, Samir M. Structure of pumpkin pectin and its effect on its technological properties. Appl Rheol. 2022;32(1):34–55.
[31] Tan T, Zhao Y, Zhao X, Chang L, Ren S. Mechanical properties of sandstone under hydro-mechanical coupling. Appl Rheol. 2022;32(1):8–21.
[32] Çilli A, Beken M, Kurt N. Determination of theoretical fracture criteria of layered elastic composite material by ANFIS method from artificial intelligence. Int J Comput Exp Sci Eng. 2022;8(2):32–9.
[33] Boodaghi Malidarre R, Akkurt İ, Gunoglu K, Akyıldırım H. Fast neutrons shielding properties for HAP-Fe_2O_3 composite materials. Int J Comput Exp Sci Eng. 2021;7(3):143–5.
[34] Şen Baykal D, Tekin H, Çakırlı Mutlu R. An investigation on radiation shielding properties of borosilicate glass systems. Int J Comput Exp Sci Eng. 2021;7(2):99–108.
[35] Safiddine S, Amokrane K, Debieb F, Soualhi H, Benabed B, Kadri E. How quarry waste limestone filler affects the rheological behavior of cement-based materials. Appl Rheol. 2021;31(1):63–75.
[36] Tekin HO, Cavli B, Altunsoy EE, Manici T, Ozturk C, Karakas HM. An investigation on radiation protection and shielding properties of 16 slice computed tomography (CT) facilities. Int J Comput Exp Sci Eng. 2018;4–2:37–40. doi: 10.22399/ijcesen.408231.